

Friction and diffusion coefficients for cooling of atoms in laser fields with multidimensional periodicity

Klaus Mølmer

Institute of Physics, Aarhus University, DK-8000 Århus C, Denmark

(Received 28 January 1991)

Methods are presented that allow numerical calculations of the friction and momentum diffusion coefficients for atomic motion in laser fields with periodicity in one, two, and three dimensions. Polarization gradients in the fields lead to increased friction on atoms with a Zeeman sublevel structure, and new features arising in the cases of motion in two and three dimensions are discussed. There is a marked position dependence of the calculated quantities, and the consequence for the forces on atoms following specified trajectories is studied. Temperatures determined from the position-averaged friction and diffusion coefficients scale with the laser power divided by the frequency detuning, except in some special configurations. Of relevance for experiments on cooling, the relative merits of four different laser configurations in three dimensions are studied.

PACS number(s): 32.80.Pj, 42.50.-p, 42.60.-v

I. INTRODUCTION

The modification of atomic motion through interaction with a laser field has been an active field of research during the recent years [1]. One of the main interests is directed towards atomic momentum spread reduction, laser cooling, which has become a powerful tool in the preparation and the maintenance of improved conditions for atomic physics experiments.

The initial proposal for laser cooling [2] was based on the Doppler effect. For a moving two-level atom, this effect implies a difference between photoabsorption rates from different plane-traveling-wave fields with the same frequency in the laboratory. With lasers tuned below the atomic transition frequency, the atom absorbs more photons from laser beams propagating opposite to its motion than from the others and a net force results, linear in velocity at low velocities. The friction coefficient is proportional to laser power in not-too-strong fields, and so is the diffusion coefficient, characteristic of heating caused by the stochastic nature of spontaneous emission processes. Steady-state velocity distributions not far from thermal ones result from the competition between friction and diffusion, and the lowest achievable temperatures are limited by the natural width of the excited atomic state (the Doppler limit) and are independent of the light intensity.

After experiments reported in 1988 [3], it has now several times been demonstrated that the Doppler limit is not the lower limit of laser cooling. The theoretical explanation was given by Dalibard *et al.* [4] and Ungar *et al.* [5], who presented detailed studies of two one-dimensional cases. Although the behavior of the friction coefficients and the diffusion coefficients is very different in the two situations, the resulting temperatures turn out to have the same dependence on field parameters, i.e., proportional to laser power divided by detuning. This is also the field dependence observed in experiments [17]. The experimental results are for cooling in three dimen-

sions, and in analogy to the simple one-dimensional cases studied, the low temperatures observed are ascribed to effects of polarization gradients in the field and the existence of several Zeeman sublevels in the lower atomic state. It is the purpose of this paper to demonstrate quantitatively that such effects are present also in two and three dimensions, and to identify the critical parameters in the cooling process.

In Sec. II, the one-dimensional cases are briefly presented, since they become useful in the interpretation of the numerical results in two and in three dimensions. The methods for calculation of the friction and diffusion coefficients for two-level atoms with general Zeeman sublevel structures (transition j_g-j_e), moving in general field configurations, are presented in Sec. III. The step from one to several dimensions introduces new properties, and some of these are discussed in Sec. IV in relation to a laser field varying in two dimensions. Some of the features were investigated recently in connection with the velocity-dependent force on a two-state atom in a particularly simple field [6]. Even more pronounced effects appear here, when cooling in fields with polarization gradients is considered. Finally, in Sec. V, numerical results of relevance for three-dimensional optical molasses are given. Friction and diffusion coefficients for atoms with a $j_g=1$ to $j_e=2$ transition interacting with four characteristic laser configurations are calculated.

II. POLARIZATION-GRADIENT COOLING MECHANISMS

The limiting temperature obtainable by laser cooling appears as the ratio between the diffusion and the friction coefficients, and this ratio is by the fluctuation-dissipation theorem proportional to the internal relaxation rate of the atom [7]. For two-state atoms the rate is the decay rate of the laser excited state Γ , and one arrives at kinetic-energy distributions with widths on the order of

the natural linewidth of the atomic transition. In the experiments mentioned above, however, the atoms have several Zeeman sublevels in the lower state (which we for simplicity shall call the ground state, although it may be an excited metastable state of the atom), and in weak fields lower internal-relaxation rates are found for redistribution of population among these states. Such a redistribution is important if the field possesses a position-dependent polarization, and in cooling experiments in three dimensions polarization gradients are unavoidable.

The role of a low relaxation rate is to give the state of a moving atom a significant delay or “lag” compared to that of an atom at rest at the same position, and thereby to increase the sensitivity of the internal state to atomic motion. Changes in the ground state can only occur through interactions with the laser, and the lag therefore becomes inversely proportional to light intensity in weak fields. Since the position-dependent mean force for a given population of the ground states is proportional to light intensity, an intensity-independent contribution is obtained for moving atoms. Unlike in the case of Doppler cooling, we thus get a friction coefficient independent of light intensity. As the intensity goes to zero, however, the velocity range over which the friction force applies diminishes. Two one-dimensional cases have been investigated in detail [4,5], in which the physical mechanisms responsible for the friction have been pointed out. These mechanisms will now be briefly reviewed.

A. Unbalanced radiation pressure, the $\sigma^+ \text{-} \sigma^-$ configuration

The first mechanism is one in which a very low atomic velocity causes a difference between the rates of photoabsorption from different plane waves which, in contrast to the Doppler mechanism, is not infinitesimal in field intensity. Such a selectivity has been suggested only for one particular laser configuration with two counterpropagating plane waves of opposite circular polarization $\sigma^+ \text{-} \sigma^-$, and it only works for atoms with a transition with $j_e = j_g + 1$, $j_g \geq 1$. The laser field is linearly polarized at all points in space, but with a position-dependent direction, and even a very low atomic velocity leads to an atomic orientation with respect to the axis of light propagation in the ground state, i.e., as a result of atomic motion, the ground-state population is transferred towards the $m = j_g$ or the $m = -j_g$ state. The oriented atom has a finite difference between the rates of absorption from the two waves; cf. the Clebsch-Gordan coefficients appearing in the coupling of different ground-excited state pairs. In the case of the $j_g = 1$ to $j_e = 2$ transition, the rates for absorption of a σ^+ and a σ^- photon by an atom nearly at rest in the $m = 1$ ground state differ by a factor of 6. A treatment including the ground-state coherences gives the friction coefficient in the $1 \rightarrow 2$ transition at low field strengths [4]

$$\alpha = \frac{120}{17} \frac{\Gamma \delta}{5\Gamma^2 + 4\delta^2} \hbar k^2. \quad (1)$$

Here, δ is the frequency detuning of the field, Γ is the natural width, and k is the wavenumber of the transition.

Note that the expression does not involve the strength of the fields.

Momentum diffusion in this configuration presents some interesting features discussed elsewhere [8]; the result for atoms at rest is independent of position and in weak fields reads [4,8]

$$D = \left[\frac{36}{17} \frac{1}{1 + 4\delta^2/5\Gamma^2} + \frac{58}{170} \right] (\hbar k)^2 s \Gamma, \quad (2)$$

which, together with the friction coefficient, leads to the expression for the temperature

$$k_B T = \frac{D}{|\alpha|} = \left[\frac{29}{300} + \frac{254}{75} \frac{\Gamma^2/4}{\delta^2 + \Gamma^2/4} \right] \frac{\hbar \kappa^2}{|\delta|}. \quad (3)$$

In Eqs. (2) and (3) we have introduced the saturation parameter s and the Rabi frequency κ for one of the traveling waves interacting with the atom for convenient parametrization of the field strength. The definitions of these quantities will be given in Sec. III. The result (3) favors weak fields and large detunings, for which the term in parentheses reduces to its initial constant.

Full quantum calculations on this configuration have shown distributions far from thermal ones [9], in agreement with calculated velocity dependences of the force and the diffusion coefficient D [8]. We shall come back to these complications in the concluding remarks.

B. Multipotential motion, the Sisyphus effect

A completely different cooling mechanism is the *Sisyphus effect*, analogous to the one occurring in stimulated molasses [10]. In weak fields, a spatial modulation of the light shifts in the ground state constitutes potentials for the atomic motion that depend upon the internal atomic state. Now, due to population transfer between ground states an atom mainly undergoes potential rises during passage of a period of the field, and there is a net transfer of kinetic into potential (atom plus field) energy. The variations of the potentials, the light shifts, are proportional to the detuning times the saturation parameter, but the weakness of the associated dipole force is compensated by the redistribution times, which are inversely proportional to saturation, and a finite friction appears. The friction depends crucially upon the mechanism of population transfer among the ground states. The following mechanisms can be identified: optical pumping, decay into uncoupled states and “nonadiabatic transitions.”

1. Pumping into states with large light-induced energy shifts

The simplest example obtains in one dimension for two counterpropagating waves with perpendicular linear polarizations [the linear perpendicular to linear (LPL) configuration] [4,5]. The field changes between linear and circular polarization along the axis of light propagation, with alternating direction of the linear polarization and sense of rotation of the circular polarization. The two ground states of the $j_g = \frac{1}{2}$ to $j_e = \frac{3}{2}$ transition experience

harmonically varying light shifts with maxima at positions with circular polarization. In points with σ^+ polarization, say, population is pumped from the $m = -\frac{1}{2}$ ground state which has a potential maximum into the $m = \frac{1}{2}$ ground state with a potential-energy minimum, when the frequency detuning is negative. As a result, a moving atom experiences a loss of kinetic energy. The friction coefficient at infinitesimal field intensity is given by a very simple expression

$$\alpha = 3 \frac{\delta}{\Gamma} \hbar k^2 . \quad (4)$$

A diffusion coefficient representing fluctuations in the dipole force on the atom has been derived [4] and reads for large detunings

$$D \simeq \frac{3}{4} (\hbar k)^2 \frac{\delta^2}{\Gamma} s . \quad (5)$$

For high detunings, the temperatures derived from Eqs. (4) and (5) are comparable to the ones derived in the σ^+ - σ^- case, in spite of the large differences between the friction and diffusion coefficients,

$$k_B T \simeq \frac{\hbar \kappa^2}{8|\delta|} . \quad (6)$$

For general j_g to $j_e = j_g + 1$ transitions the effects of coherences between ground states lead to a more complicated dependence of the friction coefficient on detuning, as shown in Fig. 1 for the $1 \rightarrow 2$ transition. However, in the limit of large detuning the result approaches Eq. (4); with higher angular momenta the proportionality with detuning remains, but with an increased coefficient. The curves were calculated by the methods to be presented in Sec. III A and III C.

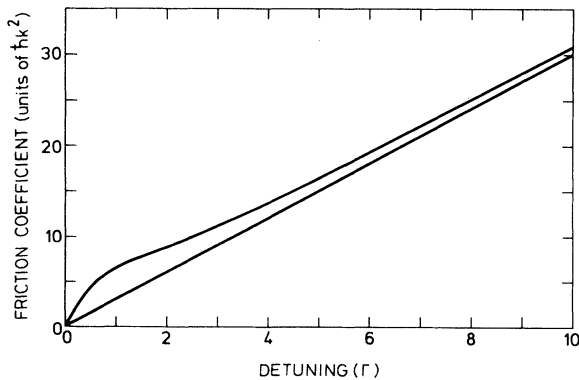


FIG. 1. Friction coefficient α for cooling in a 1D LPL configuration as a function of laser frequency detuning. The lower curve is the linear result, Eq. (4) for a $j_g = 1/2$ to $j_e = 3/2$ transition. The upper curve is the result for a $j_g = 1$ to $j_e = 2$ transition, calculated by the methods in Secs. III A and III C. The friction coefficient is an odd function of detuning.

2. Pumping into states with smaller or no light-induced energy shifts

The picture changes when $j_g = j_e$. With j_g an integer, the atom has a nonabsorbing ground state everywhere, and the friction coefficient vanishes. If j_g is a half integer, a nonabsorbing ground state only exists at points with circular light polarization. At positions of σ^\pm polarization the $m = \pm j_g$ ground state is not coupled to the field, and the population is transferred to this state, which in the case of negative detuning has the smallest (zero) light shift. The picture from above is therefore reversed, and the friction coefficient changes sign. For the $1/2 \rightarrow 1/2$ transition

$$\alpha = -3 \frac{\delta}{\Gamma} \hbar k^2 . \quad (7)$$

Also here the asymptotic proportionality with δ remains for larger j_g values, and with larger negative coefficients.

Outside the capture range of the polarization-gradient mechanism, the force must change sign and turn into the usual Doppler-cooling force, and interesting velocity distributions with narrow holes at zero velocity could be expected with this scheme.

3. "Nonadiabatic transitions" among light-shifted ground states

Since a lack of adiabaticity is germane to friction, we cannot separate a specific set of configurations with this as *the* physical mechanism. Rather, we point out that in more complex situations a contribution to the Sisyphus-effect cooling may originate in population transfer among the light shifted ground states with a more complicated interpretation. In the preceding discussion, the $m = \pm \frac{1}{2}$ ground states were always eigenstates and the mechanism was simple population transfer among them. In the general case, the diagonalization of the light shifts becomes position dependent, and a moving atom undergoes nonadiabatic transitions between the eigenstates. As experienced by the atom, the change in polarization may be so rapid that its slowly varying orientation and alignment at one moment minimizes, and at another moment maximizes, the atom-field interaction.

Cooling in the $\sigma^+ - \sigma^-$ configuration can be described by such a nonadiabaticity, but does not fall within the Sisyphus-effect cooling schemes, because the energies of the light-shifted atom-laser eigenstates do not vary with position.

III. CALCULATIONS OF FRICTION AND DIFFUSION COEFFICIENTS

The force exerted on an atom by a laser field is discussed within a semiclassical picture with the atomic position being well specified within a wavelength of the field. The corresponding quantum-mechanical uncertainty in momentum exceeds $\hbar k$. For an atom of mass M we are thus only able to treat atomic motion classically at kinetic energies above the recoil energy

$$E_{\text{rec}} = (\hbar k)^2 / 2M , \quad (8)$$

which represents a natural limit for laser cooling [11]. Equations (3) and (6) do not show this lower limit. Experiments and more detailed investigations of the LPL cooling scheme have shown that the temperatures obtained only depend on the ratio κ^2/δ , and the dependence is linear down to a value below which a rapid increase sets in. The minimum value corresponds to kinetic energies one order of magnitude above the recoil energy [12].

A. Force and friction

Within the semiclassical treatment, an ensemble of atoms located at position \mathbf{R} in a laser field experiences an average force given by the expression

$$\mathbf{f}(\mathbf{R}) = \text{Tr}[\mathbf{F}(\mathbf{R})\rho] . \quad (9)$$

Here ρ is the density matrix describing the internal atomic state of the atoms and $\mathbf{F}(\mathbf{R})$ equals minus one times the gradient of the position-dependent atom-laser interaction potential. The trace is taken within the internal atomic-state basis.

1. The atomic density matrix

We are interested in general monochromatic laser fields with spatial periodicity, and separate the classical electric field into positive and negative frequency parts

$$\mathbf{E}(\mathbf{R}, t) = \mathbf{E}(\mathbf{R})e^{-i\omega t} + \mathbf{E}^*(\mathbf{R})e^{i\omega t} . \quad (10)$$

The vector $\mathbf{E}(\mathbf{R})$ is resolved in components $E_q\epsilon_q$ with linear ($q=0$) and circular ($q=\pm 1$) polarization with respect to a fixed axis, which also defines the quantization of atomic angular momentum in the ground and excited states $|g, m\rangle, |e, m'\rangle$. In the electric dipole and rotating-wave approximation the position-dependent atom-laser interaction reads

$$\begin{aligned} H_I(\mathbf{R}) = & -d \sum_{m, q=0, \pm 1} \langle j_g m 1 q | j_e m + q \rangle \\ & \times [E_q(\mathbf{R})e^{-i\omega t} |e, m + q\rangle \\ & \times \langle g, m | + \text{H.c.}] . \end{aligned} \quad (11)$$

Here, d is the reduced atomic dipole, related to the atomic transition frequency ω_A and linewidth $\hbar\Gamma$, $\hbar\Gamma = \frac{4}{3}\omega_A^3 d^2/c^3$, $\langle j_g m 1 q | j_e m + q \rangle$ is a Clebsch-Gordan coefficient and H.c. is the Hermitian conjugate. The internal atomic part of the Hamiltonian reads

$$H_A = E_g + \hbar\omega_A \sum_{m'} |e, m'\rangle \langle e, m'| , \quad (12)$$

and the atomic density matrix is found from the optical Bloch equations

$$\frac{d\rho}{dt} = \frac{1}{i\hbar} [H_A + H_I, \rho] + S(\rho) , \quad (13)$$

where $S(\rho)$ represents terms accounting for spontaneous emission. At this point it is useful to redefine density-matrix elements between lower and upper states with a factor $\exp -i\omega t$, introducing then in the equations for the time evolution of these elements the detuning $\delta = \omega - \omega_A$

of the laser with respect to the atomic transition frequency. Equation (13) is linear in the density-matrix elements and for convenience these are arranged as elements of a vector. We use the same symbol ρ for this vector, and rewrite Eq. (13) as a matrix equation

$$\frac{d\rho}{dt} = B(\mathbf{R})\rho , \quad (13')$$

referring to the matrix B as the Bloch operator. In the Appendix, the equations for the density-matrix elements are written out explicitly.

In this paper, all laser configurations appear as superpositions of plane traveling waves propagating along the coordinate axes, with the same field strength and the same type of polarization. We define then the Rabi frequency per wave

$$\kappa = 2d|\mathbf{E}|/\hbar , \quad (14)$$

where \mathbf{E} is the positive-frequency part of the electric field in one of these traveling waves, controlled in experiments through the intensity of the laser beams. Another useful quantity is the saturation parameter

$$s = \frac{\kappa^2/2}{\delta^2 + \frac{1}{4}\Gamma^2} . \quad (15)$$

In the steady state, a two-state atom interacting with a weak plane traveling wave has an excited-state population $\pi_e = \frac{1}{2}s/(1+s) \simeq \frac{1}{2}s$, and fluoresces at a rate $\sim \frac{1}{2}s\Gamma$. These figures change only little in cases of more complex fields and atomic transitions. We use κ and s to characterize the field intensity. This unifies the description of laser cooling of all atoms with similar sublevel structure, but it should be kept in mind that the reduced dipole d , which is an atomic parameter, appears in Eq. (14).

2. Forces on slowly moving atoms

With the interaction potential in Eq. (11), the force becomes an operator in the internal state basis with matrix elements

$$\langle e, m + q | \mathbf{F}(\mathbf{R}) | g, m \rangle = d \langle j_g m 1 q | j_e m + q \rangle \nabla E_q(\mathbf{R}) e^{-i\omega t} . \quad (16)$$

Consider first an atom at rest. After the occurrence of a few spontaneous-emission processes the internal-state density matrix reaches a stationary state determined by Eq. (13') with a zero on the left-hand side. We find this stationary state by introducing the additional requirement of unit trace of the density matrix in Eq. (13'). If the p th element of ρ represents a population in the density matrix, this amounts to a substitution of the p th row in $B(\mathbf{R})$ by numbers unity multiplying populations and zero multiplying coherences in ρ , and to replacing the p th zero element on the left-hand side of Eq. (13') by unity. The equation for one of the populations in ρ has been removed, but this population is equally well derived from the value of the other populations and the normalization condition. We denote the matrix, modified in the prescribed way, by $B_p(\mathbf{R})$, and the left-hand side unit

vector by e_p , and obtain the equation for the stationary density matrix,

$$B_p(\mathbf{R})\rho^{\text{st}}(\mathbf{R})=e_p, \quad (17)$$

$B_p(\mathbf{R})$ is invertible, and its inverse $B_p^{-1}(\mathbf{R})$ will be used several times. The position-dependent force on atoms at rest now reads

$$\mathbf{f}^{\text{st}}(\mathbf{R})=\text{Tr}[\mathbf{F}(\mathbf{R})\rho^{\text{st}}(\mathbf{R})]=\text{Tr}[\mathbf{F}(\mathbf{R})B_p^{-1}(\mathbf{R})e_p]. \quad (18)$$

We use the same symbol, whether the density-matrix elements are considered as arranged in a matrix or in a vector.

Next, we consider an ensemble of very slowly moving atoms with position $\mathbf{R}=\mathbf{R}(t)$. The deviation of the density matrix from $\rho^{\text{st}}(\mathbf{R})$ appears as a lag of the internal state and to first order it is linear in velocity. This velocity dependence then also applies to the correction to the mean force. To obtain this result, we replace $d\rho/dt$ in Eq. (13') by $(\mathbf{v}\cdot\nabla)\rho(\mathbf{R})$, where \mathbf{v} is the atomic velocity. Since $B(\mathbf{R})\rho^{\text{st}}(\mathbf{R})$ vanishes, we can subtract this term on the right-hand side of Eq. (13') and obtain the equation

$$(\mathbf{v}\cdot\nabla)\rho(\mathbf{R})=B(\mathbf{R})[\rho(\mathbf{R})-\rho^{\text{st}}(\mathbf{R})]. \quad (19)$$

To find the matrix $\rho(\mathbf{R})$ to first order in \mathbf{v} , we may be replace it by its stationary value on the left-hand side, and we obtain the invertible equation

$$\sum_j v_j \left[\frac{\partial}{\partial x_j} \rho^{\text{st}}(\mathbf{R}) \right]_p = B_p(\mathbf{R})[\rho(\mathbf{R})-\rho^{\text{st}}(\mathbf{R})]. \quad (20)$$

The sum extends over the spatial coordinates, and the index p indicates that the p th element has been put equal to zero to comply with the vanishing trace of $\rho(\mathbf{R})-\rho^{\text{st}}(\mathbf{R})$. The average force at low velocities may now be written in the form

$$\mathbf{f}_v(\mathbf{R})=\mathbf{f}^{\text{st}}(\mathbf{R})+\underline{\alpha}(\mathbf{R})\mathbf{v}, \quad (21)$$

where $\underline{\alpha}(\mathbf{R})$ is a matrix with elements

$$\alpha_{ij}(\mathbf{R})=\text{Tr} \left[F_i(\mathbf{R})B_p^{-1}(\mathbf{R}) \left[\frac{\partial}{\partial x_j} \rho^{\text{st}}(\mathbf{R}) \right]_p \right]. \quad (22)$$

The velocity-dependent force is now averaged over the periodicity of the field. If all traveling plane waves appear in counterpropagating pairs of the same type and intensity, or in some other symmetric configuration, the first term in Eq. (21) averages to zero and we are left with the friction force

$$\mathbf{f}=\underline{\alpha}\mathbf{v}, \quad (23)$$

where $\underline{\alpha}$ denotes the spatial average of $\underline{\alpha}(\mathbf{R})$ defined in Eq. (22). In our numerical calculations below, Eq. (17) is solved on a grid covering a spatial period of the field in all directions. The gradient of the stationary density matrix at a given point is now most easily calculated from differences in $\rho^{\text{st}}(\mathbf{R})$ in neighboring grid points [13], and the second matrix equation is solved for each spatial derivative. The results are multiplied by the components of the force operator, and the trace is determined as indicated in Eq. (22).

B. The diffusion coefficient

The momentum diffusion coefficient is a sum of two terms D and D_{spn} resulting from the fluctuations in the force and the angular distribution of spontaneous emission. In two and three dimensions the diffusion coefficient is a tensor, but we shall only need its diagonal elements, which we calculate under the assumption of atoms at rest. For the first part, we use an expression involving two time averages of the force operator in the Heisenberg picture [7,14],

$$D_{\xi\xi}(\mathbf{R})=\int_0^\infty d\tau [\text{Re}\langle F_\xi(\mathbf{R},\tau)F_\xi(\mathbf{R},0)\rangle - \langle F_\xi(\mathbf{R})\rangle^2], \quad (24)$$

$\xi=x,y,z$.

$\langle \rangle$ denotes an ensemble average with the atom described by the stationary internal state density matrix with the vacuum modes of the field all empty. We represent the force operator by the dyads formed by atomic states, omitting for brevity the coordinate index ξ ,

$$F(\mathbf{R})=\sum_{ij} F_{ij}(\mathbf{R})|j\rangle\langle i|, \quad (25)$$

and define the Heisenberg operator

$$\Phi_{ij}(\mathbf{R},\tau)=(|j\rangle\langle i|)(\tau)[F(\mathbf{R},0)-\langle F(\mathbf{R})\rangle], \quad (26)$$

with the average value

$$\varphi_{ij}(\mathbf{R},\tau)=\langle \Phi_{ij}(\mathbf{R},\tau)\rangle. \quad (27)$$

The diffusion coefficient then rewrites

$$D(\mathbf{R})=\text{Re}\sum_{ij} F_{ij}(\mathbf{R})\int_0^\infty d\tau \varphi_{ij}(\mathbf{R},\tau). \quad (28)$$

The quantities $\varphi_{ij}(\mathbf{R},\tau)$ are useful because their time evolution, according to the quantum-regression theorem [7,14], is governed by the same equations as the expectation values of the dyads $(|j\rangle\langle i|)(\tau)$, i.e., as the internal state density matrix elements ρ_{ij} . This set of equations has already been put on a matrix form, and we arrange φ_{ij} as elements of a vector φ to obtain

$$\dot{\varphi}(\mathbf{R},\tau)=B(\mathbf{R})\varphi(\mathbf{R},\tau), \quad (29)$$

with the same $B(\mathbf{R})$ as in Eq. (13'). The integral of the vector $\int_0^\infty d\tau \varphi(\mathbf{R},\tau)$ obeys the simple equation

$$B(\mathbf{R})\int_0^\infty d\tau \varphi(\mathbf{R},\tau)=\varphi(\mathbf{R},\infty)-\varphi(\mathbf{R},0). \quad (30)$$

The atomic operators are not correlated over infinite times and the first term on the right-hand side vanishes, leaving the second one to be calculated as an expectation value in the stationary state. Equation (30) is then easily inverted with the additional constraint that φ , and therefore the integral of φ , has zero trace according to Eqs. (26) and (27),

$$\int_0^\infty d\tau \varphi(\mathbf{R},\tau)=-B_p^{-1}(\mathbf{R})\varphi(\mathbf{R},0)_p. \quad (31)$$

$B_p(\mathbf{R})$ is the same as in Sec. III A, and the index p on $\varphi(\mathbf{R},0)$ indicates again here the replacement of the p th element by zero. The diffusion coefficient is now immediately given.

To $D(\mathbf{R})$ in Eq. (28) we have to add the contribution from recoil in the spontaneous-emission processes. The distribution of photon momentum along a specific axis depends on the change of m value in the spontaneous-decay process, and the part of the diffusion coefficient is found from the excited-state population in the stationary state

$$D_{\text{spon}}(\mathbf{R}) = \frac{1}{2}\Gamma \sum_{m'} \langle e, m' | \rho^{\text{st}}(\mathbf{R}) | e, m' \rangle \times \sum_q \langle (\hbar k_\xi)^2 \rangle_q \cdot | \langle j_g m' - q | j_e m' \rangle |^2. \quad (32)$$

The variances of the projections $\hbar k_\xi$ of fluorescence photon momentum are given for example in a paper by Javanainen and Stenholm [15]. If ξ denotes a direction perpendicular to the quantization axis, $\langle (\hbar k_\xi)^2 \rangle_q$ equals $\frac{2}{5}(\hbar k)^2$ for $q=0$, and $\frac{3}{10}(\hbar k)^2$ for $q=\pm 1$.

C. The friction coefficient

Another derivation of the friction coefficient than the one described in Sec. III A can be performed [7]. For diagonal elements of the friction tensor, for example, one has

$$\alpha_{\xi\xi}(\mathbf{R}) = -\frac{2}{\hbar} \int_0^\infty d\tau \tau \text{Im} \langle F_\xi(\mathbf{R}, \tau) F_\xi(\mathbf{R}, 0) \rangle. \quad (33)$$

Since the expectation value of the Hermitian force operator is real, we can rewrite this expression as

$$\alpha_{\xi\xi}(\mathbf{R}) = -\frac{2}{\hbar} \text{Im} \sum_{ij} F_{ij}(\mathbf{R}) \int_0^\infty d\tau \tau \varphi_{ij}(\mathbf{R}, \tau). \quad (34)$$

We now apply the matrix $B(\mathbf{R})$ to the integral

$$\begin{aligned} B(\mathbf{R}) \int_0^\infty d\tau \tau \varphi(\mathbf{R}, \tau) &= \int_0^\infty d\tau \tau \dot{\varphi}(\mathbf{R}, \tau) \\ &= [\tau \varphi(\mathbf{R}, \tau)]_0^\infty - \int_0^\infty d\tau \varphi(\mathbf{R}, \tau) \\ &= - \int_0^\infty d\tau \varphi(\mathbf{R}, \tau). \end{aligned}$$

The last term has just been calculated in Eq. (31), and we can again use the zero trace of $\varphi(\mathbf{R}, \tau)$ to provide an invertible equation so that

$$\int_0^\infty d\tau \tau \varphi(\mathbf{R}, \tau) = -B_p^{-1}(\mathbf{R}) \left[\int_0^\infty d\tau \varphi(\mathbf{R}, \tau) \right]_p, \quad (35)$$

and the friction coefficient comes immediately from Eq. (34). Slowly moving atoms, passing through all points in space, can now be described by a friction coefficient which is the position average of Eq. (34).

The calculation of the friction coefficient just outlined might seem more accurate than the one discussed in Sec. III A, since it does not require the calculation of spatial derivatives. These can, however, be obtained to any desired accuracy through an increase in the number of points covering the spatial periodicity of the field. Also, it might be a bit misleading that the same symbol $B_p(\mathbf{R})$ was used throughout. For the calculations in Sec. III A the Hermiticity of the density operator, $\rho_{ij} = \rho_{ji}^*$, implies a reduction in the number of equations to be considered

by a factor of 2. No such reduction is found for the φ_{ij} 's, the steady-state mean values of the non-Hermitian operators Φ_{ij} , and for the transition $j_g=1$ to $j_e=2$ the size of the matrix $B_p(\mathbf{R})$ is 128×28 in a real representation, as compared to 64×64 in Sec. III A. Since the computing time for solving linear equations scales as the number of unknowns cubed, the formulation in Sec. III C is only useful when also the diffusion coefficient is required. Then the friction coefficient follows almost without additional work.

IV. FORCE, FRICTION, AND DIFFUSION IN TWO DIMENSIONS

We shall now study some of the additional effects appearing in two and three dimensions, and for that purpose we consider a laser configuration of two plane standing waves intersecting at right angles and with perpendicular linear polarizations. The positive-frequency part of the electric field vector is taken on the form

$$\mathbf{E}(\mathbf{R}) = 2E [\cos(kx)\epsilon_y + e^{i\phi}\cos(ky)\epsilon_z], \quad (36)$$

where ϵ_y and ϵ_z are unit vectors in the y and z directions, and ϕ is a phase which, according to Eq. (10), causes a time lag ϕ/ω between maxima in the real field amplitudes along ϵ_y and ϵ_z . We shall in the following discuss divergences in the friction coefficient, the velocity dependence of the force, and the relevance of controlling the phase difference ϕ , which has not yet been done in experimental investigations. For this particular configuration changes in ϕ have tremendous effect on the values of the friction and diffusion coefficients.

A. $\alpha(\mathbf{R})$ diverges in the vicinity of field nodes

The largest contributions to the mean friction matrix come from positions with large field variations, i.e., from the field nodes. If we put $\phi=\pi/2$ in Eq. (36), we get a field which is σ^+ polarized with respect to the x axis, σ_x^+ , along the line $kx=ky$, and σ_x^- polarized along the line $ky=\pi-kx$. These two lines intersect in $kx=ky=\pi/2$, which is a node for the total electric field. On the line $ky=\pi/2$ the field is linearly polarized along ϵ_y, π_y , and on the line $kx=\pi/2$ the polarization is π_z ; see Fig. 2(a). For motion along any one of these lines, the atoms experience no polarization gradient and hence a vanishing force at very low field strengths. As an example, the friction matrix element $\alpha_{xx}(\mathbf{R})$ also vanishes on these lines except on the one with $kx=\pi/2$. Here, it reaches very large values in the vicinity of a field node. The reason is that near the node the atom moving parallel to the x axis experiences a rapid change of field polarization between σ_x^+ and σ_x^- . The spatial derivative of ρ^{st} and, according to Eq. (22), α_{xx} diverge as one divided by the distance to the node. This is illustrated in Fig. 2(b), where $-\alpha_{xx}$ is plotted as a function of position within the dashed frame in part (a) of the figure for the atomic transition $j_g=1$ to $j_e=2$. The field parameters are $\delta=-2\Gamma$,

$\kappa = 2d|E|/\hbar = \Gamma$. This is not exactly the weak-field limit, but in the vicinity of the field node the position-dependent Rabi frequency becomes very small. The rather arbitrary peak values in the figure are $|\alpha_{xx}| \sim 1.5 \times 10^4 \hbar k^2$ at a distance $k\Delta y \sim 0.02$ from the field node. With a finer grid, larger values are obtained.

The convergence properties of the mean friction matrix are not affected by the local divergences, but in the numerical calculations extra attention must be paid to these regions. In the evaluations presented below, a finer grid is therefore defined near field nodes. To ensure the numerical stability of the matrix inversions, we are allowed to increase the Rabi frequency in the calculations provided we scale the resulting stationary position-dependent force and the diffusion coefficient with the same factor squared. These quantities are both well behaved everywhere. The friction coefficient is independent of κ . The range in velocities over which the force is linear diminishes with the increase in α , and the force on a moving atom remains finite.

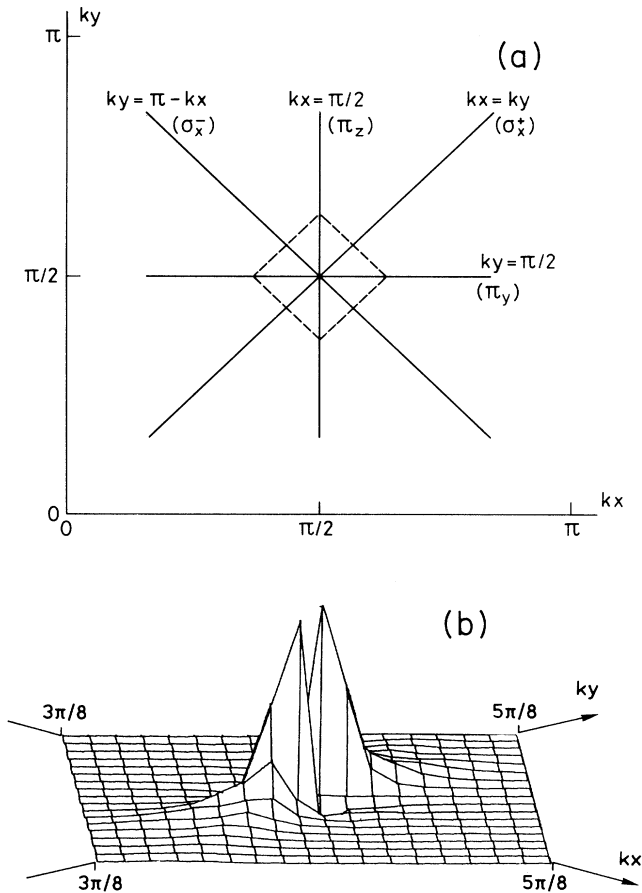


FIG. 2. (a) Lines in the xy plane with constant polarization; see text. The field is given in Eq. (36) with $\phi = \pi/2$. (b) The component $-\alpha_{xx}$ of the friction matrix as a function of position within the dashed frame in (a). The atomic transition is $j_g = 1$ to $j_e = 2$, the detuning is -2Γ , and the Rabi frequency equals Γ .

B. Force on a moving atom

For an atomic ensemble following a given trajectory $\mathbf{R}(t)$, the instantaneous mean force can be calculated from Eq. (9) if ρ has been found by integration of Eq. (13'). After the occurrence of a few spontaneous decays, $\rho(t)$ becomes independent of the initial state, and if the trajectory is such that the atom experiences a periodic interaction Hamiltonian, the density matrix evolves into a steady state with the same periodicity. This situation prevails for rectilinear motion at constant speed in directions characterized by integer coordinates, and the fact that any direction is arbitrarily close to such a direction was used recently in the development of a method for calculating forces on atoms moving with arbitrary velocities in general field configurations [6]. A mean force was then introduced as the average of Eq. (9) over one period of the atom-field interaction. In Fig. 3 are plotted the components of this force perpendicular to (upper curve) and parallel with (lower curve) the trajectory which passes in the direction (2,1) through the origin where both standing waves have an antinode. A positive perpendicular force component implies a counterclockwise deflection of the atomic velocity. The field configuration and parameters are as in Fig. 2. The position-averaged friction is isotropic, i.e., $\underline{\alpha}$ is proportional to the identity matrix, and has the value $\alpha = -12.7 \hbar k^2$. The inset of Fig. 3 shows the low-velocity region with the isotropic result (only component parallel to velocity) indicated by a dashed line. The force corresponding to the trajectory $x = 2y$ is clearly not in agreement with this result, and the reason is that α is determined as an average over all points in space. If we average $\underline{\alpha}(\mathbf{R})$ over the trajectory $x = 2y$ only, we find $\langle F_{\parallel}, F_{\perp} \rangle_{x=2y} = v(-5.8, 0.75) \hbar k^2$. The expressions for

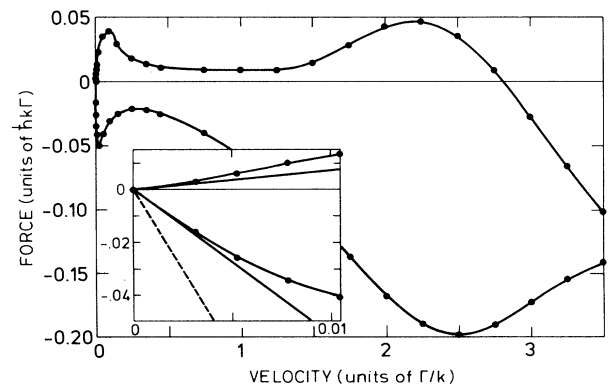


FIG. 3. The force as a function of velocity along the line $x = 2y$. All parameters are the same as in Fig. 2. The figure shows the components of the force perpendicular to (upper curve) and parallel with (lower curve) the particle velocity. Inset: A comparison of the force components in the low-velocity domain and the friction result. The dashed line is the position averaged isotropic result for the force (only longitudinal component), the solid lines are results based on calculations along the line $x = 2y$ only.

the parallel and perpendicular components are illustrated in the inset by solid lines, and are in much better agreement with the calculated force.

In an experiment it may be more realistic to assume a uniform spatial distribution of atoms moving in a specified direction, i.e., on a set of parallel trajectories. The relevant friction then becomes the average of $\underline{\alpha}(\mathbf{R})$. In symmetric field configurations this quantity is proportional to the identity matrix, and there is no risk of an accumulation of particles along special directions where a localization on preferred trajectories could invalidate the mean results. The use of the averaged friction matrix here may therefore be even better justified than the use of the position averaged force in Ref. [6].

C. Importance of phase difference between waves

1. The friction coefficient

After the spatial average over parallel trajectories, there is no force perpendicular to the motion when this is along the axis directions. This result, which is valid for all field configurations of the type studied in this paper, follows from the observation that a change of sign of x or y causes a change of sign of the x or y component of the force without modification of the density matrix. Since the vectors $(v,0)$ and $(0,v)$ are eigenvectors, the matrix $\underline{\alpha}$ is diagonal. Note that this does not exclude transverse force components; for motion at an angle Θ to the x axis, we get from Eq. (23) the force components parallel and perpendicular to the velocity

$$\begin{aligned} F_{\parallel} &= [\cos^2\Theta\alpha_{xx} + (\sin^2\Theta)\alpha_{yy}]v, \\ F_{\perp} &= (\cos\Theta)(\sin\Theta)(\alpha_{yy} - \alpha_{xx})v. \end{aligned} \quad (37)$$

If α_{xx} and α_{yy} are different, the atomic motion is deflected towards one of the coordinate axes. In highly symmetric field configurations α_{xx} and α_{yy} have no reason to differ, and they do not. This is the situation for the field configurations studied in Sec. V.

As observed in Ref. [6], the phase relation between the different field components plays a decisive role for the forces on atoms moving in the laser field. In Fig. 4(a) the two components α_{xx} and α_{yy} are shown as functions of the phase ϕ for atoms with a $j_g=1$ to $j_e=2$ transition. The Rabi frequency is 0.1Γ and the detuning is 2Γ . A change of sign of the detuning *and of the phase difference* leads to a change of sign of α_{xx} and α_{yy} . The two components are identical when ϕ is a multiple of $\pi/2$ since there is a trivial exchange symmetry between x and y or $(\pi/k - y)$ in these cases. Otherwise the two fields do not interact with the atoms with the same efficiency, and the symmetry is broken, as we observe from the difference between the two curves in the figure. For some values of ϕ and a smaller detuning, even α_{xx} and α_{yy} of opposite signs were obtained.

More prominent in Fig. 4(a) is the effect of the phase variation on the absolute value of the friction coefficient. The order-of-magnitude reduction of the friction as ϕ changes from $\pi/2$ to 0 or π can be explained in terms of a complete change in the cooling mechanism. When

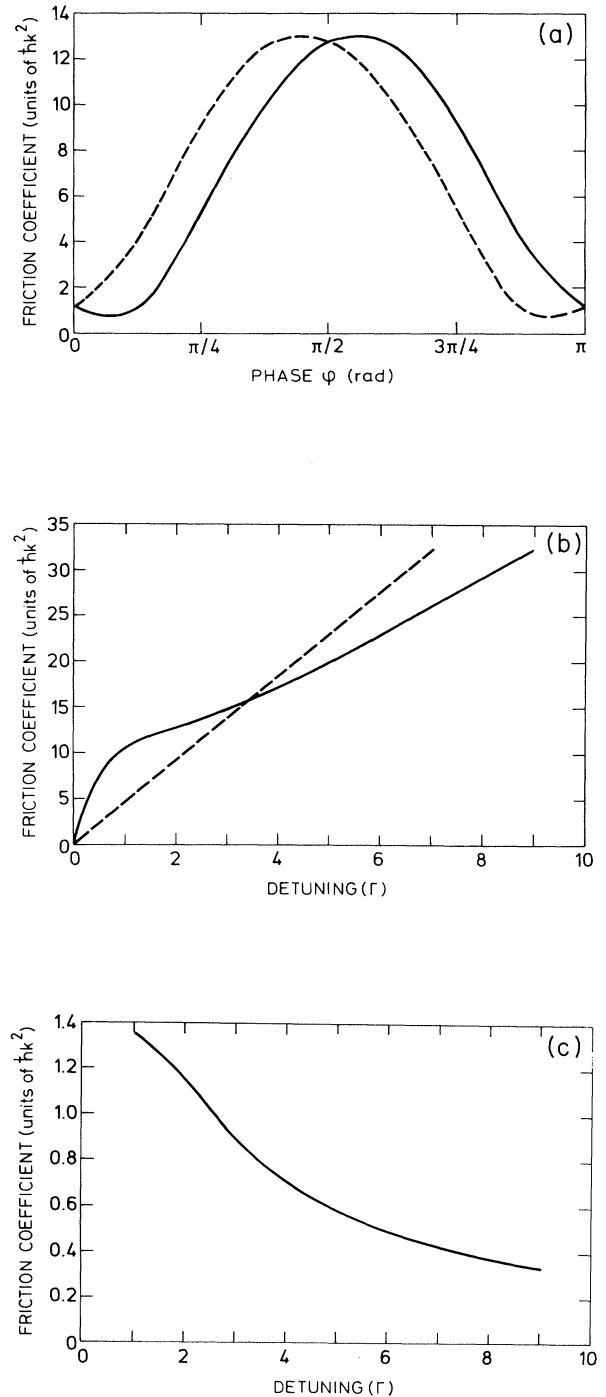


FIG. 4. (a) The position-averaged components α_{xx} (solid curve) and α_{yy} (dashed curve) of the (diagonal) friction matrix as function of phase ϕ . The transition is $j_g=1$ to $j_e=2$, $\delta=2\Gamma$, and $\kappa=0.1\Gamma$. (b) Detuning dependence of $\alpha_{xx}=\alpha_{yy}$ for $\phi=\pi/2$. $\kappa=0.1\Gamma$ and the atomic transitions are $j_g=1$ to $j_e=2$ (solid curve) and $j_g=1/2$ to $j_e=3/2$ (dashed curve). (c) Detuning dependence of $\alpha_{xx}=\alpha_{yy}$ for $\phi=0$. $\kappa=0.1\Gamma$ and the atomic transition is $j_g=1$ to $j_e=2$. The friction coefficient is proportional to intensity (negligible) for the $j_g=1/2$ to $j_e=3/2$ transition.

$\phi = \pi/2$, the two linearly polarized fields are out of phase, and as we have seen, the resulting field is circularly polarized at some points in space. We thus obtain a Sisyphus-effect mechanism similar to the one described in Sec. II B 1. When the fields are in phase, $\mathbf{E}(\mathbf{R})$ in Eq. (36) is real everywhere and the total field is linearly polarized but with a position-dependent direction and magnitude. For a $j_g = \frac{1}{2}$ to $j_e = \frac{3}{2}$ transition there is in this case no difference between the light-shifted ground-state energies, and at low field strengths the stationary density matrix becomes independent of position. There is then no lag of the internal state at low velocities and the friction becomes proportional to intensity. In contrast, with a $j_g = 1$ to $j_e = 2$ transition, atoms experience a polarization-gradient force of which part might be of the same origin as in the one-dimensional (1D) $\sigma^+ - \sigma^-$ configuration of Sec. II A, but the main contribution remains of the Sisyphus-effect type ("nonadiabatic transitions"). The repopulation mechanism is not nearly as effective as for circularly polarized light and the force becomes much weaker than for $\phi = \pi/2$. In Figs. 4(b) and 4(c) the detuning dependence of $\alpha_{xx} = \alpha_{yy}$ is shown for the $j_g = 1$ to $j_e = 2$ case, with $\phi = \pi/2$ and 0. Indeed, the difference between the two graphs points to completely different mechanisms. The results for $\phi = \pi/2$ have the asymptotic proportionality to detuning, but the coefficients have changed as compared to Fig. 1. The dashed curve in Fig. 4(b) is for the $j_g = \frac{1}{2}$ to $j_e = \frac{3}{2}$ case. The detuning dependence is more complicated when $\phi = 0$.

The strong variation with the temporal phase is not general for all laser configurations. It is observed also with $\sigma^+ - \sigma^-$ configurations along the two axes, where the field is linearly polarized everywhere when the relative phase is a multiple of π . In the other fields studied, positions with elliptic or circular polarization components cannot be avoided and the variation of α with ϕ is less dramatic.

Also at higher field strengths and at finite velocities the phase difference is important [6] and it should be possible to perform experiments, where the phase ϕ is controlled, to confirm this. Beam deflection may be a better probe than laser cooling, since as we shall see below the effect on the cooling force also shows up in the diffusion coefficient in a way that makes the final distributions of cooled samples less sensitive to ϕ .

2. Diffusion coefficient and temperature

The average diffusion coefficients D_{xx} and D_{yy} have been calculated in the symmetric cases $\phi = 0, \pi/2$ where they are identical, and they also show characteristics of different cooling mechanisms. We take also here the value $\kappa = 0.1\Gamma$ for the Rabi frequency and plot in Fig. 5 the dependence of D_{xx} on detuning for the $j_g = 1$ to $j_e = 2$ atomic transition. When $\phi = \pi/2$, we expect D_{xx} to be proportional to $\delta^2 s \propto \kappa^2$ at large detunings as in Eq. (5), i.e., not to vary with detuning, and this is indeed observed to be the case. When $\phi = 0$, the mechanism differs from the one in Sec. II B 1, and the reduced friction is accompanied by a reduction in the diffusion coefficient.

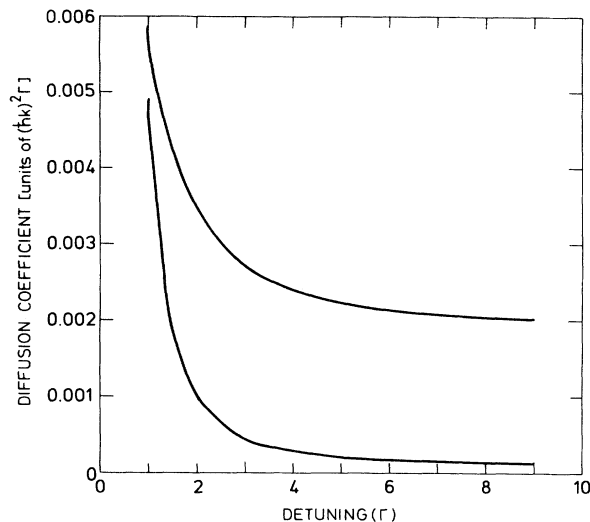


FIG. 5. Diffusion coefficient (including D_{spont}) as a function of detuning. The transition is $j_g = 1$ to $j_e = 2$, $\kappa = 0.1\Gamma$. The upper curve is for $\phi = \pi/2$, the lower one is for $\phi = 0$. The diffusion coefficient is an even function of detuning.

A temperature characterizing stationary cooled distributions may now be obtained under the assumption that the distributions stay within the velocity range where the linear friction result (23) applies, and where the diffusion coefficient does not differ significantly from its value at zero velocity. In symmetric configurations the same temperature may be assigned to each velocity component

$$k_B T = k_B T_x = D_{xx} / |\alpha_{xx}|. \quad (38)$$

From the quantities calculated above, we obtain the temperature as a function of the field parameters. In the 1D examples, temperatures scale with κ^2/δ , the dependence on Rabi frequency coming from the diffusion coefficient, and in Fig. 6 we study $k_B T / (\hbar\kappa^2/|\delta|)$ as a function of the negative detuning for both choices of the phase $\phi = \pi/2$ and 0. A constant is only obtained for $\phi = \pi/2$.

In cooling experiments fast compared to the time scale on which ϕ varies (mechanical vibrations can impose fluctuations in the value of ϕ on a msec time scale), the measured temperatures are expected to scatter between the two curves. If the phase varies significantly during the experiment, e.g., because the cooling effect is too weak to be applied over shorter times, some mean value would result. It is an appealing possibility to actually control the phase in the experiment; in the configuration studied, this could change the result by a factor of $\gtrsim 2$.

Apart from the requirements of a linear force and a constant diffusion coefficient, the results rely on the validity of our semiclassical description, i.e., that the width of the calculated distribution corresponds to energies larger than the recoil energy in Eq. (8). Cooling to temperatures in the vicinity of E_{rec}/k_B should be described in a complete quantum manner as in Refs. [9] and [12]. The heavier the atomic species, the better a semiclassical treatment is.

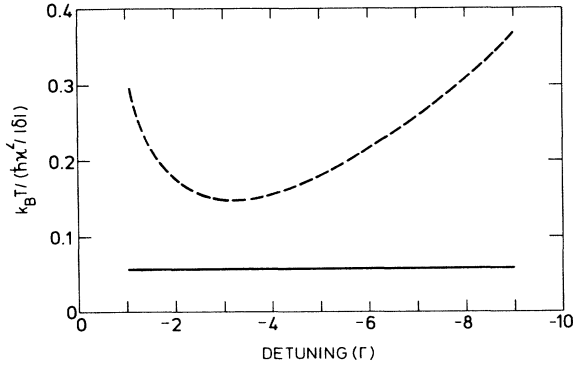


FIG. 6. $k_B T / (\hbar \kappa^2 / |\delta|)$ as a function of (negative) detuning for a $j_g=1$ to $j_e=2$ transition. $\kappa=0.1\Gamma$, and the phase ϕ equals $\pi/2$ (solid curve) and zero (dashed curve).

V. NUMERICAL RESULTS FOR 3D MOLASSES

The relative merits of four different laser configurations with all of the waves in phase are studied. The configurations are obtained as superpositions of waves propagating along all three coordinate axes, and they are all symmetric with respect to permutations of the position coordinates. The field configurations are the following.

(a) Linearly polarized plane standing waves

$$\mathbf{E}(\mathbf{R}) = 2E [\cos(kx)\epsilon_y + \cos(ky)\epsilon_z + \cos(kz)\epsilon_x], \quad (39a)$$

(b) $\sigma^+ - \sigma^-$ configuration along all axes

$$\begin{aligned} \mathbf{E}(\mathbf{R}) = E (e^{ikx}\epsilon_{+1}^{(x)} + e^{-ikx}\epsilon_{-1}^{(x)} + e^{iky}\epsilon_{+1}^{(y)} \\ + e^{-iky}\epsilon_{-1}^{(y)} + e^{ikz}\epsilon_{+1}^{(z)} + e^{-ikz}\epsilon_{-1}^{(z)}), \end{aligned} \quad (39b)$$

(c) circularly polarized plane standing waves

$$\mathbf{E}(\mathbf{R}) = 2E [\cos(kx)\epsilon_{+1}^{(x)} + \cos(ky)\epsilon_{+1}^{(y)} + \cos(kz)\epsilon_{+1}^{(z)}], \quad (39c)$$

(d) LPL configuration along all axes

$$\begin{aligned} \mathbf{E}(\mathbf{R}) = E (e^{ikx}\epsilon_y + e^{-ikx}\epsilon_z + e^{iky}\epsilon_z \\ + e^{-iky}\epsilon_x + e^{ikz}\epsilon_x + e^{-ikz}\epsilon_y). \end{aligned} \quad (39d)$$

The unit vectors of circular polarization with respect to the x and y axes can be obtained by cyclic permutation of the coordinate indices of the conventional vectors $\epsilon_{\pm 1} = \epsilon_{\pm 1}^{(z)} = \mp (1/\sqrt{2})(\epsilon_x \pm i\epsilon_y)$.

In the configurations (a) and (b), the polarization is linear everywhere but the electric vector varies in magnitude and direction. In the configurations (c) and (d), circular polarization with respect to different directions is present at different positions in the field. Qualitatively,

we therefore expect the results to show the same two types of behavior as obtained in Sec. IV with $\phi=0$ and $\pi/2$.

The calculations were performed on a $28 \times 28 \times 28$ mesh covering a cube of wavelength size, and with the replacement of grid points in field nodes by a small $6 \times 6 \times 6$ mesh on the corresponding volume element. A further increase in the density of grid points modifies the results on the percent level only.

The results of the numerical calculations are presented

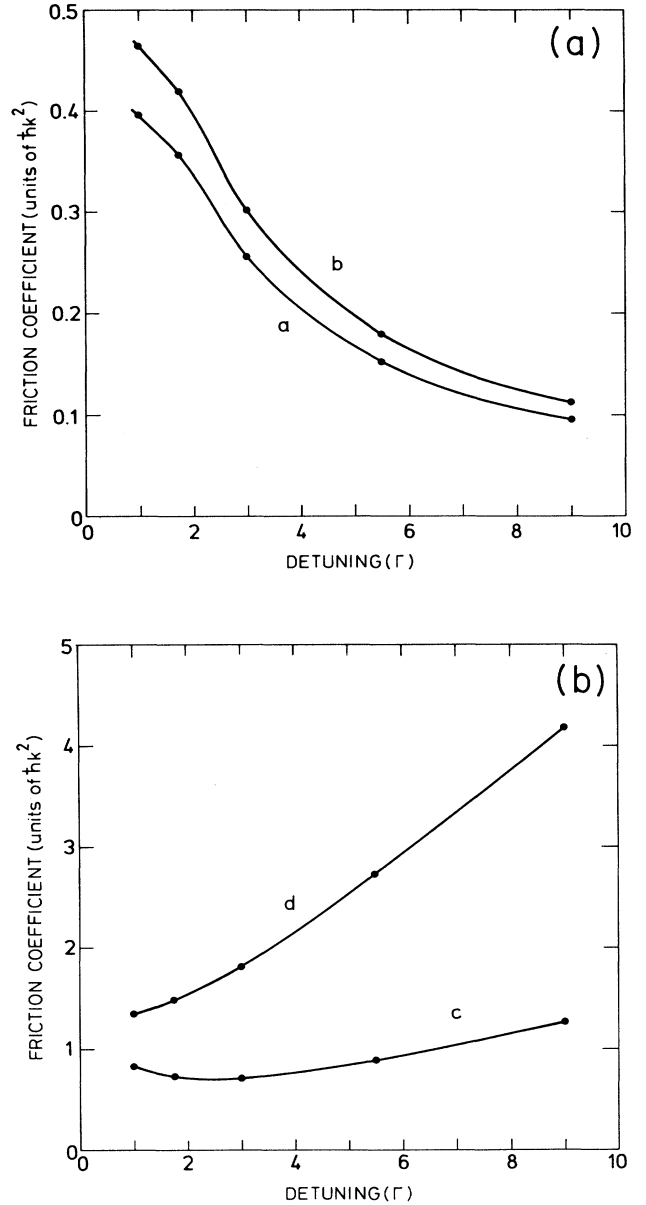


FIG. 7. Friction coefficients as functions of detuning. The two first configurations (labeled a and b) are represented in (a), the other two (c and d) in (b). The transition is $j_g=1$ to $j_e=2$, $\kappa=0.1\Gamma$.

as functions of the frequency detuning. The Rabi frequency per traveling plane wave equals 0.1Γ , and the transition is $j_g=1$ to $j_e=2$. Figure 7 shows friction coefficients in qualitative agreement with Figs. 4(b) and 4(c). The diffusion coefficients are shown in Fig. 8. The curves are practically indistinguishable for configurations (a) and (b). In general, the laser configuration with the stronger friction also shows the larger diffusion coefficients.

The temperatures defined as the ratio between D and $|\alpha|$ are presented in Fig. 9. The results for configurations (a) and (b) on the one hand and (c) and (d) on the other show for large detunings an asymptotic proportionality to $\hbar\kappa^2/\Gamma$ and $\hbar\kappa^2/|\delta|$, respectively. Phase variations in configurations (a) and (b) change the result completely. In Sec. IV C it was demonstrated how sensitive the friction and diffusion coefficients are to the relative phase of the fields. The results presented for the configurations (a) and (b) in this section are only valid if the mutual phases of the fields are controlled in the experiments, otherwise an average of the results over those phases should be made. In Fig. 4(a) we observe that such an average will be dominated by the results obtained with a nonzero phase difference, which are shown in Figs. 4(b), 5, and 6 to behave qualitatively like the 1D results with temperatures proportional to $\hbar\kappa^2/|\delta|$. In the configurations (c) and (d) D and α change also, but the resulting temperature is only weakly affected. If the fields propagating along the z axis are in quadrature with the others in configuration (c), we obtain at $\delta=-9\Gamma$ the result indicated by an open circle in Fig. 9. Experiments have been performed on Cs by Salomon *et al.* [17]. With configurations (a) and (d), but without controlling the relative phases of the six incoming laser beams, these authors obtained temperatures proportional to $\hbar\kappa^2/|\delta|$. This agrees with our expectations. Our results for

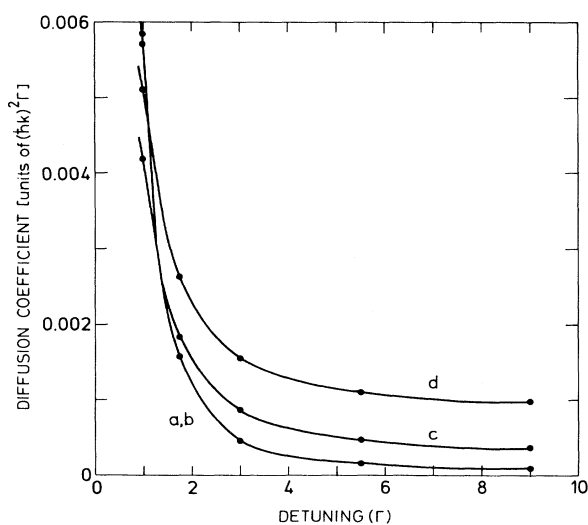


FIG. 8. Diffusion coefficients as functions of detuning. The letters beside the curves refer to the four different configurations studied. The transition is $j_g=1$ to $j_e=2$, $\kappa=0.1\Gamma$.

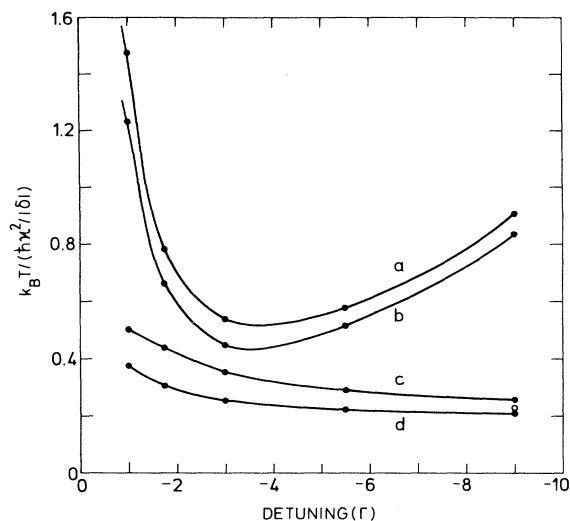


FIG. 9. $k_B T / (\hbar\kappa^2/|\delta|)$ as a function of detuning for the four laser configurations. The transition is $j_g=1$ to $j_e=2$, $\kappa=0.1\Gamma$. The open circle indicates the result if the fields propagating along the z axis in configuration (c) are in quadrature with the others.

configuration (d) are about a factor of 1.5 lower than those obtained in the experiments on Cs atoms by Salomon *et al.* [17]. However, theoretical temperatures obtained with the actual $j_g=4$ to $j_e=5$ transition in Cs may deviate from the $j_g=1$ to $j_e=2$ results presented in this paper.

VI. DISCUSSION

A semiclassical treatment of atomic motion in laser fields with multidimensional periodicity has been given. Means have been presented for numerical calculations of the position-dependent force to first order in velocity, and of the position-dependent diffusion coefficient. Instead of solving a Fokker-Planck equation on the position-momentum phase space, we averaged the calculated quantities over position and disregarded localization effects. New aspects appearing in two and three dimensions were discussed.

It has been demonstrated that polarization gradients imply intensity-independent friction coefficients for multilevel atoms, and that laser cooling in three dimensions can lead to temperatures below the Doppler limit. This was expected from one-dimensional studies [4,5], and the dependence of temperature on the field parameters was found to agree with experiments [17] and with these 1D calculations, except in some cases where a different cooling mechanism was suggested as an explanation of the deviations. Only for special configurations, and only with special values of the relative phase of the laser beams are these deviations important, and they may be relevant only in experiments specially aimed at studying them. As a two-dimensional example, collimation of a thermal beam may be considered. An effect on the

transverse width and shape of the beam after the interaction with the lasers should be observable with the technique developed in depth, e.g., in Ref. [18].

A temperature can only be unambiguously defined when the cooled velocity distribution is Gaussian. The temperature is then given by the ratio of the diffusion and friction coefficients, and the heavier the atom the narrower the velocity distribution, and the better justified is our assumption of a force linear in velocity and a constant diffusion coefficient. In Ref. [12] it was shown that the velocity dependence of the force and diffusion coefficient can deviate from these assumptions and still lead to thermal distributions, but here we do not enter a discussion of velocity-dependent diffusion coefficients.

The temperatures given in this paper are proportional to the intensity of the laser beams. Consistency of our treatment, however, imposes two lower limits.

(i) Velocity distributions with $\langle v^2 \rangle$ proportional to intensity are assumed to stay within the range where the polarization gradient force is linear in velocity. The extent of this range is proportional to intensity [4], and therefore a lower intensity limit exists.

(ii) We have used a semiclassical treatment that is valid for kinetic energies sufficiently above the recoil energy, Eq. (8). Full quantum calculations should be performed in order to examine polarization gradient cooling when this limit is approached, and they will probably lead to

distributions with atomic momenta of the order of a few times the photon momentum as in the 1D examples [9,12].

Finally, we mention also that cooling of atoms in uniform magnetic fields, and of three-level atoms interacting with two different laser frequencies, can be treated with the formalism presented. These are two recent additional suggestions for cooling to temperatures below the Doppler limit [19,20].

ACKNOWLEDGEMENT

Constructive criticism on the manuscript by E. Bonderup is gratefully acknowledged.

Note added in proof. In two dimensions a nonlinear and anisotropic dependence of the position-averaged force on low velocities, which is not revealed by the procedures in Sec. III for calculating the friction matrix, may result from the reduction in velocity capture range near field nodes. The author is grateful to V. Finkelstein and P. Berman for bringing this result to his attention prior to the publication of their analytical work on a special configuration.

APPENDIX: THE OPTICAL BLOCH EQUATIONS

The density matrix equations (13) in the paper are the following [16]:

$$\begin{aligned} \frac{d}{dt} \langle g, m | \rho | g, m' \rangle = & -i \sum_{q=-1}^1 \left[\frac{dE_q}{\hbar} \langle j_g m' 1 q | j_e m' + q \rangle \langle g, m | \rho | e, m' + q \rangle - \frac{dE_q^*}{\hbar} \langle j_g m 1 q | j_e m + q \rangle \langle e, m + q | \rho | g, m' \rangle \right] \\ & + \Gamma \sum_{q=-1}^1 \langle j_g m 1 q | j_e m + q \rangle \langle j_g m' 1 q | j_e m' + q \rangle \langle e, m + q | \rho | e, m' + q \rangle, \end{aligned} \quad (\text{A1})$$

$$\begin{aligned} \frac{d}{dt} \langle e, m | \rho | g, m' \rangle = & i \sum_{q=-1}^1 \frac{dE_q}{\hbar} (\langle j_g m - q 1 q | j_e m \rangle \langle g, m - q | \rho | g, m' \rangle \\ & - \langle j_g m' 1 q | j_e m' + q \rangle \langle e, m | \rho | e, m' + q \rangle) + (-\frac{1}{2}\Gamma + i\delta) \langle e, m | \rho | g, m' \rangle, \end{aligned} \quad (\text{A2})$$

$$\frac{d}{dt} \langle g, m | \rho | e, m' \rangle = \frac{d}{dt} \langle e, m' | \rho | g, m \rangle^*, \quad (\text{A3})$$

$$\begin{aligned} \frac{d}{dt} \langle e, m | \rho | e, m' \rangle = & i \sum_{q=-1}^1 \left[\frac{dE_q}{\hbar} \langle j_g m - q 1 q | j_e m \rangle \langle g, m - q | \rho | e, m' \rangle \right. \\ & \left. - \frac{dE_q^*}{\hbar} \langle j_g m' - q 1 q | j_e m' \rangle \langle e, m | \rho | g, m' \rangle \right] - \Gamma \langle e, m | \rho | e, m' \rangle. \end{aligned} \quad (\text{A4})$$

With Eqs. (A1)–(A4) it is possible to write down the (sparse) matrix $B(\mathbf{R})$ used throughout the paper.

- [1] See, for example, the special issues of J. Opt. Soc. Am. B **2**, 1706 (1985); **6**, 2019 (1989).
 [2] T. W. Hänsch, A. L. Schawlow, Opt. Commun. **13**, 68 (1975).

- [3] P. D. Lett, R. N. Watts, C. I. Westbrook, W. D. Phillips, P. L. Gould, and H. J. Metcalf, Phys. Rev. Lett. **61**, 169 (1988).
 [4] J. Dalibard, C. Salomon, A. Aspect, E. Arimondo, R.

- Kaiser, N. Vansteenkiste, and C. Cohen-Tannoudji, in *Proceedings of the 11th Conference on Atomic Physics*, edited by S. Haroche, J. C. Gay, and G. Grynberg (World Scientific, Singapore 1989); J. Dalibard and C. Cohen-Tannoudji, *J. Opt. Soc. Am. B* **6**, 2023 (1989).
- [5] P. J. Ungar, D. S. Weiss, E. Riis, and S. Chu, in *Proceedings of the 11th Conference on Atomic Physics* (Ref. [4]); *J. Opt. Soc. Am. B* **6**, 2058 (1989).
- [6] K. Mølmer, K. Berg-Sørensen, and E. Bonderup, *J. Phys. B* **24**, 2327 (1991).
- [7] J. Dalibard and C. Cohen-Tannoudji, *J. Phys. B* **18**, 1661 (1985); J. Dalibard, *Phys. Scr.* **T12**, 28 (1986).
- [8] Y. Castin and K. Mølmer, *J. Phys. B* **23**, 4101 (1990).
- [9] Y. Castin, K. Mølmer, J. Dalibard, and C. Cohen-Tannoudji, in *Laser Spectroscopy IX, 1989*, edited by M. Feld, A. Mooradian, and J. Thomas (Academic, New York, 1990).
- [10] J. Dalibard and C. Cohen-Tannoudji, *J. Opt. Soc. Am. B* **2**, 1707 (1985).
- [11] Cooling below the recoil limit has been discussed by A. Aspect, E. Arimondo, R. Kaiser, N. Vansteenkiste, and C. Cohen-Tannoudji, *J. Opt. Soc. Am. B* **6**, 2112 (1989); H. Wallis and W. Ertmer, *ibid.* **6**, 2211 (1989); and by K. Mølmer, *Phys. Rev. Lett.* **66**, 2301 (1991). The first suggestion makes use of a “dark resonance”; the second uses a multichromatic field and the third a pulsed field acting on a narrow atomic transition [$(\hbar k)^2/2M > \hbar\Gamma$], and they all require a full quantum treatment of the atomic motion.
- [12] Y. Castin, J. Dalibard, and C. Cohen-Tannoudji, in *Light Induced Kinetic Effects on Atoms, Ions and Molecules, 1990*, edited by L. Moi, S. Gozzini, C. Gabbanini, E. Arimondo, and F. Strumia (ETS Editrice, Pisa, 1991).
- [13] The spatial derivative of $\rho^{\text{st}}(\mathbf{R})$ is found by use of a four-point interpolation formula, cf. *Handbook of Mathematical Functions*, Natl. Bur. Stand. Appl. Ser. No. 55, edited by M. Abramowitz and I. A. Stegun (U.S. GPO, Washington, DC, 1965).
- [14] J. P. Gordon and A. Ashkin, *Phys. Rev. A* **21**, 1606 (1980).
- [15] J. Javanainen and S. Stenholm, *Appl. Phys.* **21**, 35 (1980).
- [16] C. Cohen Tannoudji, in *Frontiers in Laser Spectroscopy*, Les Houches, Session XXVII, edited by R. Balian, S. Haroche, and S. Lieberman (North-Holland, Amsterdam 1977), Vol. 1.
- [17] C. Salomon, J. Dalibard, W. D. Phillips, A. Clairon, and S. Guellati, *Europhys. Lett.* **12**, 683 (1990).
- [18] B. Sheehy, S.-Q. Shang, R. Watts, S. Hatamain, and H. Metcalf, *J. Opt. Soc. Am. B* **6**, 2165 (1989).
- [19] B. Sheehy, S.-Q. Shang, P. van der Straten, S. Hatamian, and H. Metcalf, *Phys. Rev. Lett.* **64**, 858 (1990).
- [20] V. G. Minogin, M. A. Olshany, and S. V. Shulga, *J. Opt. Soc. Am. B* **6**, 2108 (1989).